

# Dimensionality of the spatio-temporal entanglement of PDC photon pairs

A. Gatti<sup>1,2</sup>, T. Corti<sup>2</sup>, E. Brambilla<sup>2</sup>,

<sup>1</sup> *Istituto di Fotonica e Nanotecnologie del CNR, Piazza L. Da Vinci 32, Milano, Italy;* <sup>2</sup> *Dipartimento di Scienza e Alta Tecnologia dell'Università dell'Insubria, Via Valleggio 11, Como, Italy*

D.B.Horoshko

*Laboratoire PhLAM, Université de Lille 1, 59655 Villeneuve d'Ascq, France and  
B.I.Stepanov Institute of Physics, NASB, Nezavisimosti Ave. 68, Minsk 220072 Belarus*

In this work the Schmidt number of the two-photon state generated by parametric-down conversion (PDC) is evaluated in the framework of a fully spatio-temporal model for PDC. A comparison with the results obtained in either purely spatial or purely temporal models shows that the degree of entanglement of the PDC state cannot be trivially reduced to the product of the Schmidt numbers obtained in models with lower dimensionality, unless the detected bandwidth is very narrow. This result is a consequence of the non-factorability of the state in the spatial and temporal degrees of freedoms of twin photons. In the limit of a broad pump beam, we provide a geometrical interpretation of the Schmidt number, as the ratio between the volume of the phase matching region and of a correlation volume.

## Introduction

The process of parametric down-conversion (PDC) occurring in a nonlinear crystal is a widely employed source of entangled photons, which are ubiquitous ingredients in modern quantum technologies. An appealing aspect of this source is the possibility of generating *high-dimensional entanglement*, both in the sense that entanglement is generated in various degrees of freedom of the photon pair (polarization, time-energy, position-momentum), and because spatial and temporal entanglement is realized in a high-dimensional Hilbert space, due to the naturally ultrabroad bandwidths of the process. High dimensional entanglement is attracting more and more attention, because of its potential to increase the capacity and the security of quantum communication channels, and the precision of quantum metrological techniques [1].

In this context an obvious question concerns the effective dimensionality of the entanglement of the PDC state (or alternatively the number of entangled modes generated by the process), usually quantified by the so-called *Schmidt number* [2, 3]. Traditional approaches typically concentrate on a single degree of freedom at a time, depending on the application considered. For example, the dimensionality of the temporal entanglement has been evaluated in various configurations, including spontaneous PDC [4, 5], quantum frequency combs generated by a synchronously pumped optical parametric oscillator [6, 7], waveguided PDC [8]. The degree of transverse spatial entanglement of PDC [9, 10, 15] is of paramount importance for assessing both the dimensionality of the orbital angular momentum entanglement (see e.g. [11–16]) and the resolution of quantum imaging techniques [17]. In these studies a net separation between the spatial and temporal degrees of freedom was often justified by the assumption of a narrow filtering in the neglected degree of freedom.

However, as for many nonlinear optical processes, PDC is ruled by phase matching, which imposes an angular dispersion relation linking the frequencies and the angles of emission of the generated photons in a non-factorable way. This implies a strong coupling between temporal and spatial degrees of freedom, which has been recently evidenced by the so called *X-entanglement* [18–22], a feature shown for example by type I biphotons in conditions close to collinear phase matching, whose temporal delays and the transverse spatial displacements at the crystal exit face are linked by a proportionality relation (corresponding to an X-shape of the spatio-temporal correlation in any plane containing time and one transverse coordinate). The space-time coupling is often regarded as a negative feature, because it affects e.g. the purity of the purely spatial entanglement when temporal degrees of freedom are neglected [23]. However, it also represents a valuable resource for engineering the quantum state of biphotons, since the spatial degrees of freedom can be used to tailor the temporal entanglement [18, 19] in order e.g. to realize an ultrabroadband temporally entangled state [21].

In this work we adopt a fully spatio-temporal model of PDC, in order to investigate the effect of the non-factorability of the state in space and time on the dimensionality of the biphoton entanglement. We shall concentrate on the evaluation of the spatio-temporal Schmidt number of PDC entanglement in the ultra-low gain regime of PDC <sup>1</sup>

---

<sup>1</sup> The Schmidt decomposition of the state in the full spatio-temporal domain is very hard to achieve (even numerically), due to the

Based on a general formula for the Schmidt number, which involves integrals in 12 and 6 dimensions, we both obtain numerical evaluations and analytical results, the latter being valid when the profile of the pump driving the process is broad enough. In the same limit, we introduce a useful geometric interpretation of our results, which shows that the Schmidt number quantifying entanglement is basically the ratio between the volume of the region where phase matching efficiently occurs and a correlation volume, thus being proportional to the number of spatio-temporal correlated modes.

The same methods of analysis are used to calculate the Schmidt number in a purely 2D spatial model and in a purely 1D temporal model of PDC. An important result that will be demonstrated is that the Schmidt dimensionality of the 3D model of PDC cannot be trivially reduced to the product of the Schmidt numbers in the models of lower dimensionality. As a matter of fact, the Schmidt dimensionality of the full PDC state is by far larger than what would be expected from an approach that considers space and time as separable degrees of freedoms, showing that an enormous number of entangled modes is available for the down-converted light. This result is again a consequence of the intrinsic non-factorability of the state in its spatial and temporal degrees of freedom, and shows that using a full spatio-temporal model for describing PDC is essential in order to correctly quantify the degree of entanglement of the state.

The results presented in this work extend and complement those presented in [25], where a 2D spatio-temporal model (1 temporal dimension +1 spatial dimension) for PDC has been investigated.

## I. STARTING POINT

In [18, 19, 24] the spatio-temporal quantum properties of the PDC light were described by studying the evolution of the quantum field operators through the nonlinear crystal, and deriving input-output relations linking the operators at the crystal output face with those at the entrance face. Here we consider the equivalent state-formalism, in which the state evolves from the input to the output face of the crystal. We focus on type I PDC, in the regime of ultra-low gain where the probability of generating a photon pair in each spatio-temporal mode is small (more precisely, the probability of generating more than one photon pair in each mode is negligible). The output biphoton quantum state can thus be written as a generic superposition of the vacuum state  $|0\rangle$  and of a state with two photons generated in all possible spatio-temporal modes:

$$|\psi_{\text{PDC}}\rangle = |0\rangle + \int d\vec{w}_1 \int d\vec{w}_2 \mathcal{C}(\vec{w}_1, \vec{w}_2) A^\dagger(\vec{w}_1) A^\dagger(\vec{w}_2) |0\rangle \quad (1)$$

where  $A$  is the quantum field operators for the down-converted field, and  $\vec{w}$  indicates the full 3-D spatio-temporal Fourier coordinate with the short-hand notation

$$\vec{w} = (\vec{q}, \Omega), \quad (2)$$

where  $\vec{q}$  is the transverse component of the photonic wave-vector  $\vec{q} = (q_x, q_y)$ , with respect to the mean propagation direction  $z$  of the pump field, and  $\Omega = \omega - \omega_p/2$  is the temporal frequency shift from the central frequency of the PDC emission. The coordinate in the direct transverse space-time domain will be denoted by

$$\vec{\xi} = (\vec{x}, t), \quad (3)$$

where  $\vec{x} = (x, y)$  is the spatial coordinate spanning the transverse plane at the crystal exit face, and  $t$  is time, with the convention

$$\vec{w} \cdot \vec{\xi} = \vec{q} \cdot \vec{x} - \Omega t. \quad (4)$$

$\mathcal{C}(\vec{w}_1, \vec{w}_2)$  in Eq.(1) is the probability amplitude of generating a photon pair in the spatio temporal modes  $\vec{w}_1$  and  $\vec{w}_2$ , and can be determined by exploiting the equivalence with the field formalism developed in [18, 19, 24]. In these references the biphoton amplitude was calculated in terms of the field-field correlation at the crystal output face

$$\psi(\vec{w}_1, \vec{w}_2) = \langle A(\vec{w}_1, l_c) A(\vec{w}_2, l_c) \rangle \quad (5)$$

$$= \frac{g}{(2\pi)^{\frac{3}{2}}} \tilde{\mathcal{A}}_p(\vec{w}_1 + \vec{w}_2) \text{sinc} \frac{\Delta(\vec{w}_1, \vec{w}_2)}{2} e^{i \frac{\Delta(\vec{w}_1, \vec{w}_2)}{2}} \quad (6)$$

where

---

hyperbolic geometry of the phase matching relations. However, the Schmidt number can be computed even without performing the decomposition.

- $A(\vec{w}, l_c)$  is the output field operator, and the expectation in Eq.(5) is taken on the input vacuum state;
- $g$  is the dimensionless gain parameter, proportional to the pump peak amplitude, the crystal length and the nonlinear susceptibility;
- $\tilde{\mathcal{A}}_p$  is the Fourier transform of the pump beam profile at the crystal exit face:

$$\tilde{\mathcal{A}}_p(\vec{w}) := \int \frac{d\vec{\xi}}{(2\pi)^{3/2}} \mathcal{A}_p(\vec{\xi}) e^{-i\vec{\xi} \cdot \vec{w}}, \quad (7)$$

where normalization is such that  $\mathcal{A}_p(\vec{\xi} = 0) = 1$ ;

- $\Delta$  is the phase matching function, which accounts for the conservation of longitudinal momentum in the microscopic PDC process

$$\Delta(\vec{w}_1, \vec{w}_2) = [k_{sz}(\vec{w}_1) + k_{sz}(\vec{w}_2) - k_{pz}(\vec{w}_1 + \vec{w}_2)] l_c \quad (8)$$

$k_{sz}$  being the longitudinal component of the (ordinary) signal wave vector,  $k_{pz}$  the analogous quantity for the (extraordinary) pump, and  $l_c$  the crystal length.

We remark that the right hand side of Eq.(6) is the first order term in the parameter  $g$  of a perturbative expansion of the full solution of the propagation equation of field operators in the nonlinear crystal, so that expression (6) is valid only in the very low gain regime  $g \ll 1$ . Similarly, as it is well-known, the right hand side of Eq.(1) shows the zeroth and first order terms in  $g$  of a perturbative expansion of the full PDC state.

By using the equivalence between the two formalisms, and by calculating the field correlation on the generic output state (1) we also obtain:

$$\begin{aligned} \psi(\vec{w}_1, \vec{w}_2) &= \langle \psi_{\text{PDC}} | A(\vec{w}_1, 0) A(\vec{w}_2, 0) | \psi_{\text{PDC}} \rangle \\ &= \mathcal{C}(\vec{w}_1, \vec{w}_2) + \mathcal{C}(\vec{w}_2, \vec{w}_1) = 2\mathcal{C}(\vec{w}_1, \vec{w}_2). \end{aligned} \quad (9)$$

where we used the symmetry properties of the state. Thus the two-photon state has the well known form

$$|\psi_{\text{PDC}}\rangle = |0\rangle + \frac{1}{2} \int d\vec{w}_1 \int d\vec{w}_2 \psi(\vec{w}_1, \vec{w}_2) A^\dagger(\vec{w}_1) A^\dagger(\vec{w}_2) |0\rangle \quad (10)$$

with the biphoton amplitude  $\psi$  being given by (6).

Apart from the biphoton amplitude, the other quantity of interest is the coherence function of the signal field, which after long but simple calculations can be derived from (10) as:

$$G(\vec{w}, \vec{w}') := \langle \psi_{\text{PDC}} | A^\dagger(\vec{w}) A(\vec{w}') | \psi_{\text{PDC}} \rangle \quad (11)$$

$$= \int d\vec{w}_2 \psi^*(\vec{w}, \vec{w}_2) \psi(\vec{w}', \vec{w}_2) \quad (12)$$

From this equation, the total number of PDC photons is obtained as

$$\begin{aligned} N &= \int d\vec{w}_1 \langle \psi_{\text{PDC}} | A^\dagger(\vec{w}_1) A(\vec{w}_1) | \psi_{\text{PDC}} \rangle \\ &= \int d\vec{w}_1 \int d\vec{w}_2 |\psi(\vec{w}_1, \vec{w}_2)|^2 \end{aligned} \quad (13)$$

In type I PDC a signal and an idler fields are in principle not distinguishable. A bipartition of the system can be introduced in various ways, for example by sorting photons depending on their propagation directions (positive or negative with respect to any transverse axis) [22], which, however, is a good bipartition only in the case of a very broad pump waist, when twin photons are always created with symmetric transverse wave-vectors  $\pm \vec{q}$ . In the ultra-low gain regime where at most a single photon pair at a time is detected, a very general bipartition is obtained by simply considering the two output modes of a symmetric beam-splitter

$$\begin{aligned} A_1(\vec{w}) &= \frac{1}{\sqrt{2}} [A(w) + i a_v(\vec{w})] \\ A_2(\vec{w}) &= \frac{1}{\sqrt{2}} [i A(w) + a_v(\vec{w})] \end{aligned} \quad (14)$$

where  $a_v$  is a vacuum field operator. By substituting in the state (10) the inverse of (14) one gets two terms that describe creation of two photons into each of the output modes 1 and 2 of the beam-splitter, and a term that creates one photon in mode 1 and one photon in mode 2. Following the literature treating the degree of entanglement in PDC [4, 5, 9, 10], we shall consider rather than the full PDC, the state vector conditioned to the measurement of a photon pair (the vacuum and two-photon terms are dropped). Assuming that detectors are placed at the two output modes, and coincidences are detected, the state conditioned to the appearance of a coincidence takes the form (a part from global normalization factors)

$$|\phi\rangle = \int d\vec{w}_1 \int d\vec{w}_2 \psi(\vec{w}_1, \vec{w}_2) A_1^\dagger(\vec{w}_1) A_2^\dagger(\vec{w}_2) |0\rangle_1 |0\rangle_2 \quad (15)$$

The degree of entanglement of such a conditional state has been investigated in previous literature in the purely temporal [4, 5] or purely spatial [9, 10, 15] domains.

## II. THE SCHMIDT NUMBER OF PDC ENTANGLEMENT: INTEGRAL FORMULA

A good quantifier of the degree of entanglement for continuous variable pure states is the so-called Schmidt number, defined as the inverse of the purity of the state of each separate subsystem

$$\mathcal{K} = \frac{1}{\text{Tr}\{\rho_1^2\}} \quad (16)$$

where  $\rho_1$  is the reduced density matrix of the subsystem 1. In connection with the Schmidt decomposition of the PDC conditional state, the Schmidt number is recognized to give an estimate of the number of Schmidt modes participating in the entanglement, i.e. of the effective dimensionality of the entanglement [10].

We will derive an integral formula for the Schmidt number in the case of the conditional state (15), similar to what obtained in Refs.[5], [15]. First of all the state (15) is not normalized,

$$\langle\phi|\phi\rangle = \int d\vec{w}_1 \int d\vec{w}_2 |\psi(\vec{w}_1, \vec{w}_2)|^2 = N \quad (17)$$

From the system conditional density matrix

$$\rho = \frac{|\phi\rangle\langle\phi|}{\langle\phi|\phi\rangle} \quad (18)$$

the reduced density matrix of the subsystem 1 can be calculated (Appendix A) as

$$\begin{aligned} \rho_1 &= \text{Tr}_2\{\rho\} \\ &= \frac{1}{N} \int d\vec{w}_1 \int d\vec{w}'_1 G(\vec{w}'_1, \vec{w}_1) A_1^\dagger(\vec{w}_1) |0\rangle_1 \langle 0|_1 A_1(\vec{w}'_1). \end{aligned} \quad (19)$$

Notice that in the limit where the coherence function becomes a Dirac-delta - i.e in the limit of a monochromatic plane-wave pump- the reduced density matrix becomes a sum of projectors onto 1-photon states.

Next we calculate the purity of such a reduced state:

$$\text{Tr}_1\{\rho_1^2\} = \frac{1}{N^2} \left[ \int d\vec{w}_1 \int d\vec{w}'_1 |G(\vec{w}_1, \vec{w}'_1)|^2 \right] \quad (20)$$

An integral formula for the Schmidt number can be therefore written as:

$$\mathcal{K} = \frac{N^2}{B} \quad (21)$$

where

$$B = \int d\vec{w}_1 \int d\vec{w}'_1 |G(\vec{w}_1, \vec{w}'_1)|^2 \quad (22)$$

$$\begin{aligned} &= \int d\vec{w}_1 \int d\vec{w}_2 \int d\vec{w}'_1 \int d\vec{w}'_2 [\psi(\vec{w}_1, \vec{w}_2) \psi(\vec{w}'_1, \vec{w}'_2) \\ &\quad \psi^*(\vec{w}_1, \vec{w}'_2) \psi^*(\vec{w}'_1, \vec{w}_2)] \end{aligned} \quad (23)$$

and  $N$  is given by Eq.(17).

### III. THE NEARLY PLANE-WAVE PUMP APPROXIMATION

In order to evaluate the Schmidt number of the two-photon state from formula (21) we face the problem of calculating the 6-dimensional and 12-dimensional integrals involved in the calculation of  $N$  and  $B$ , respectively. These integrations can be numerically performed, but in the following we will provide more transparent results based on the approximation of a broad enough pump profile.

Let us come back to the expression(6) for the biphoton amplitude that we rewrite as

$$\psi'(\vec{w}_1, \vec{w}_2) = \tilde{\mathcal{A}}_p(\vec{w}_1 + \vec{w}_2)V(w_1, w_2) \quad (24)$$

$$V(w_1, w_2) = \text{sinc} \frac{\Delta(\vec{w}_1, \vec{w}_2)}{2} e^{i \frac{\Delta(\vec{w}_1, \vec{w}_2)}{2}} \quad (25)$$

where  $\Delta$  is the phase matching function defined in Eq. (8), and we got rid of the constant  $g/(2\pi)^{3/2}$  that factors out in the ratio  $\mathcal{K} = N^2/B$ . We now introduce the pump spectral coordinates  $\vec{w}_p = \vec{w}_1 + \vec{w}_2 := (\vec{q}_p, \Omega_p)$ . Provided that  $\sigma_p$  is the transverse waist of the pump beam at the output crystal face, and  $\tau_p$  its duration, the pump Fourier transform  $\tilde{\mathcal{A}}_p$  dies out on the scales  $\delta q_p = 2/\sigma_p$ ,  $\delta \Omega_p = 2/\tau_p$ . This claim is exactly true for a Gaussian pump profile

$$\mathcal{A}_p(\vec{x}, t) = e^{-x^2/\sigma_p^2} e^{-t^2/\tau_p^2} \quad (26)$$

$$\tilde{\mathcal{A}}_p(\vec{q}_p, \Omega_p) = \frac{\sigma_p^2 \tau_p}{2^{3/2}} e^{-q_p^2 \sigma_p^2/4} e^{-\Omega_p^2 \tau_p^2/4} \quad (27)$$

The function  $V$  is strongly peaked along the curve where phase matching takes place. As elaborated in detail in the Appendix B of [19], for a broad enough pump the variation of this function with respect to the pump spectral coordinates can be neglected. In other words,  $V(w_1, -\vec{w}_1 + \vec{w}_p)$  does not vary significantly with  $\vec{w}_p$  on the scale over which the pump Fourier profile dies out:

$$\begin{aligned} \tilde{\mathcal{A}}_p(\vec{w}_p)V(\vec{w}_1, -w_1 + \vec{w}_p) &\approx \tilde{\mathcal{A}}_p(\vec{w}_p)V(\vec{w}_1, -\vec{w}_1) \\ &:= \tilde{\mathcal{A}}_p(\vec{w}_p)V(\vec{w}_1) \end{aligned} \quad (28)$$

We call this approximation nearly plane wave pump (NPWP) approximation. It is based on making a Taylor expansion of  $V$  in power series of the pump variables  $\vec{w}_p$ , and on finding the conditions under which the first order terms of the expansion can be neglected with respect to the zeroth order term [19]. These conditions can be summarized as:

$$\tau_p \gg \tau_{GVM} = \left| \frac{l_c}{v_{gs}} - \frac{l_c}{v_{gp}} \right| \quad (29)$$

$$\sigma_p \gg l_{walk-off} = \left| l_c \frac{\partial k_p}{\partial q_x} \right|. \quad (30)$$

Here  $\tau_{GVM}$  is the maximum delay time between the signal and the pump wave in crossing the nonlinear crystal, due to the mismatch between the group velocities  $v_{gs}, v_{gp}$  of the ordinary signal and extraordinary pump.  $l_{walk-off}$  is the maximum lateral walk-off between the two waves, associated to tilt of the Poynting vectors. In the example of a 4mm BBO crystal, pumped at a wavelength  $\lambda_p = 527\text{nm}$ , we have  $\tau_{GVM} \approx 500\text{fs}$ ,  $l_{walk-off} \approx 250\mu\text{m}$ , so that the NPWPA is within the reach of practical experimental generation of PDC photon pairs.

The use of this limit simplifies remarkably the expression (21) of the Schmidt number. As reported in detail in the Appendix B, the integral formula (21) takes the form

$$\mathcal{K} = \frac{N^2}{B} \rightarrow \frac{\left[ \int d\vec{\xi}_p |\mathcal{A}_p(\vec{\xi}_p)|^2 \right]^2}{\int d\vec{\xi}_p |\mathcal{A}_p(\vec{\xi}_p)|^4} \frac{\left[ \int d\vec{w} |V(\vec{w})|^2 \right]^2}{(2\pi)^3 \int d\vec{w} |V(\vec{w})|^4}. \quad (31)$$

The integrals involving the pump coordinates can now be readily performed. By assuming a Gaussian pump profile as in (26), we easily obtain:

$$\mathcal{K} = \frac{\int d\vec{w} |V(\vec{w})|^2}{\int d\vec{w} |V(\vec{w})|^4} \frac{\int d\vec{w} \text{sinc}^2 \frac{\Delta(\vec{w})}{2}}{\pi^{\frac{3}{2}} \frac{4}{\sigma_p^2} \frac{2}{\tau_p}}. \quad (32)$$

As we shall see in the following, under rather general conditions <sup>2</sup> the first term at r.h.s. of Eq.(32) is a purely numerical factor, namely

$$\frac{\int d\vec{w} |V(\vec{w})|^2}{\int d\vec{w} |V(\vec{w})|^4} \approx \frac{3}{2}. \quad (33)$$

. Thanks to this circumstance, the result of Eq.(32) has a transparent geometrical interpretation. The term  $\int d\vec{w} \text{sinc}^2 \frac{\Delta(\vec{w})}{2}$  can be interpreted as the volume of the region in the  $(\vec{q}, \Omega)$  3D space where phase matching occurs, since the  $\text{sinc}^2$  function has a sharp maximum where  $\Delta(\vec{q}, \Omega) = 0$  (see Fig.1). This corresponds to the portion of the  $(\vec{q}, \Omega)$  space where the probability of photon-pair production is not negligible.

On the other side the quantity at denominator is (a part from numerical factors) the spectral volume of the pump  $\delta q_p^2 \delta \Omega_p = \frac{4}{\sigma_p^2} \frac{2}{\tau_p}$ . This quantity defines the **correlation volume**, i.e. the size the of the correlated modes, because the expression (24) tells us that in the NPWPA, the width of the biphoton correlation as a function of  $\vec{w}_1 + \vec{w}_2$  is determined by the pump Fourier profile. Thus  $\delta q_p^2 \delta \Omega_p$  represents the uncertainty in the determination of the transverse wave vector  $\vec{q}_2$  and frequency  $\Omega_2$  of a photon, once the transverse wave vector  $\vec{q}_1$  and frequency  $\Omega_1$  of its twin have been determined. Therefore  $\mathcal{K}$  is on the order of the ratio:

$$\mathcal{K} \propto \frac{\text{volume of the phase matching region}}{\text{correlation volume}} \quad (34)$$

and can be interpreted as the number of correlated modes participating to the state. The formula (34) gives us a simple geometric interpretation of the Schmidt number, which will be very useful in understanding some results.

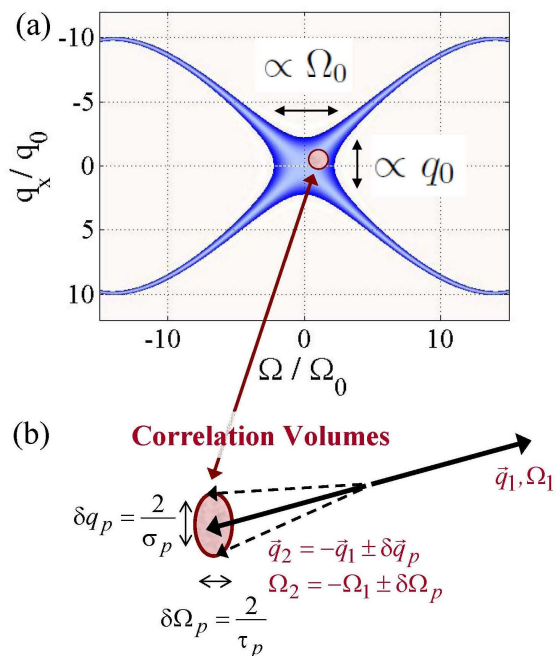


FIG. 1: Geometrical interpretation of the Schmidt number. The figure plots a) the phase matching region in the  $(q_x, \Omega)$  plane, here defined by  $|V(\vec{q}, \Omega)|^2 > 0.1$  (the full 3D volume has a biconical shape), and b) the correlation volumes, which in the 3D picture would be Gaussian bullets of size determined by the spectral estension  $\delta q_p^2 \delta \Omega_p$  of the pump. Case of a 4 mm type I BBO crystal, pumped at  $\lambda_0 = 527\text{nm}$  for collinear phase matching.

<sup>2</sup> this conditions amount to requiring that phase matching occurs within the spectral region considered, a conterexample being provided in Section VI

#### IV. SCHMIDT NUMBER OF 3D X-ENTANGLED BIPHOTONS

We can proceed further, and find an analytical approximation of the Schmidt number result of Eq.(32) in the NPWPA. To this end, we need to calculate integrals over the phase matching curves of the form  $\int d\vec{w}|V(\vec{w})|^2$ ,  $\int d\vec{w}|V(\vec{w})|^4$ . Our calculations are based on the use of two further approximations (in additions to the NPWPA):

i) The first approximation consists in a quadratic expansion of the phase mismatch function with respect to  $q$  and  $\Omega$ , equivalent to adopting the paraxial and quadratic dispersion approximations:

$$\Delta(q, \Omega) = \Delta_0 l_c - \frac{q^2}{q_0^2} + \frac{\Omega^2}{\Omega_0^2} \quad (35)$$

where  $\Delta_0 = 2k_s - k_p$  is the collinear phase mismatch at degeneracy, and

$$q_0 = \sqrt{\frac{k_s}{l_c}}, \quad (36)$$

$$\Omega_0 = \sqrt{\frac{1}{k_s'' l_c}}, \quad (37)$$

with  $k_s = k_s(0)$ ,  $k_s'' = d^2 k_s / d\Omega^2|_0$ . This expansion is strictly valid only for small  $\Omega$  (close to degeneracy) and small  $q$ . For the remaining of this section we assume conditions of *collinear* phase matching,  $\Delta_0 l_c \approx 0$ , where the phase matching curve in the plane  $(q, \Omega)$  has the characteristic hyperbolic geometry shown in Fig.1. The parameters  $q_0$ , associated to spatial diffraction and  $\Omega_0$ , associated to group velocity dispersion (GVD), define the typical variation scales of  $|V(\vec{w})|^2$  along  $q$  and  $\Omega$ , respectively. In the example of the 4 mm BBO crystal, their values are  $q_0 \approx 5 \times 10^{-2} \mu\text{m}^{-1}$ ,  $\Omega_0 \approx 0,76 \times 10^{14} \text{Hz}$ .

ii) The second approximation consists in substituting the  $\text{sinc}^2\left(\frac{\Delta(\vec{w})}{2}\right)$  with a box function, with the same value of the indefinite integral

$$\text{sinc}^2\left(\frac{\Delta(\vec{w})}{2}\right) \rightarrow \chi_\alpha\left(\frac{\Delta(\vec{w})}{2}\right) = \begin{cases} \frac{\pi}{\alpha} & \frac{\Delta(\vec{w})}{2} \in \left(-\frac{\alpha}{2}, \frac{\alpha}{2}\right) \\ 0 & \text{elsewhere} \end{cases} \quad (38)$$

which satisfies  $\int \text{sinc}^2(x) dx = \int \chi_\alpha(x) dx = \pi$ . Here the parameter  $\alpha$  can be used in principle as a fitting parameter. Approximation (38) seems very rough, but it turned out surprisingly accurate: the rationale behind this result is that the  $\text{sinc}^2$  has a sharp peak where  $\Delta(\vec{w}) = 0$ , and in order to evaluate its integral in the 3D space it is more important to take into account the geometrical shape of the curve where its maximum lies rather than the detailed shape of the peak. Figure 2 compares the box function approximation to the true phase matching function in the example of the BBO crystal. Here, substantial deviations appear at large values of  $\Omega$  and  $q$  because of the failure of the quadratic approximation for phase matching.

Notice that if we also assume that  $|V(\vec{w})|^4$  can be approximated by the box function  $\chi_\alpha^2(\vec{w})$ , with the request that, this time,

$$\int dx \chi_\alpha^2(x) = \frac{\pi^2}{\alpha} = \int dx \text{sinc}^4(x) = \frac{2}{3}\pi, \quad (39)$$

we find the correct value of  $\alpha = \frac{3}{2}\pi$ . This also shows that, within these approximations, the ratio

$$\frac{\int d\vec{w}|V(\vec{w})|^2}{\int d\vec{w}|V(\vec{w})|^4} \approx \frac{\int d\vec{w}\chi_\alpha(\vec{w})}{\int d\vec{w}\chi_\alpha^2(\vec{w})} = \frac{\alpha}{\pi} = \frac{3}{2} \quad (40)$$

The box function approximation allow us to evaluate easily the integrals over the phase matching curves inside Eq. (32). In this evaluation, we assume that our model describes a measurement performed over a large but limited spectral bandwidth  $\Omega \in (-\Omega_{max}, \Omega_{max})$ . For simplicity, here we do not pose limits to the spatial bandwidth (which will be instead done in the following section) . After some calculations we obtain the two different results depending on the detected bandwidth  $\bar{\Omega}_{max} = \frac{\Omega_{max}}{\Omega_0}$ :

- **small bandwidth result** ( $\bar{\Omega}_{max} < \sqrt{\alpha}$ )

$$\mathcal{K} = \frac{\alpha}{4} \sqrt{\frac{\alpha}{\pi}} q_0^2 \Omega_0 \sigma_p^2 \tau_p \left[ \frac{\bar{\Omega}_{max}}{\sqrt{\alpha}} + \frac{1}{3} \left( \frac{\bar{\Omega}_{max}}{\sqrt{\alpha}} \right)^3 \right], \quad (41)$$

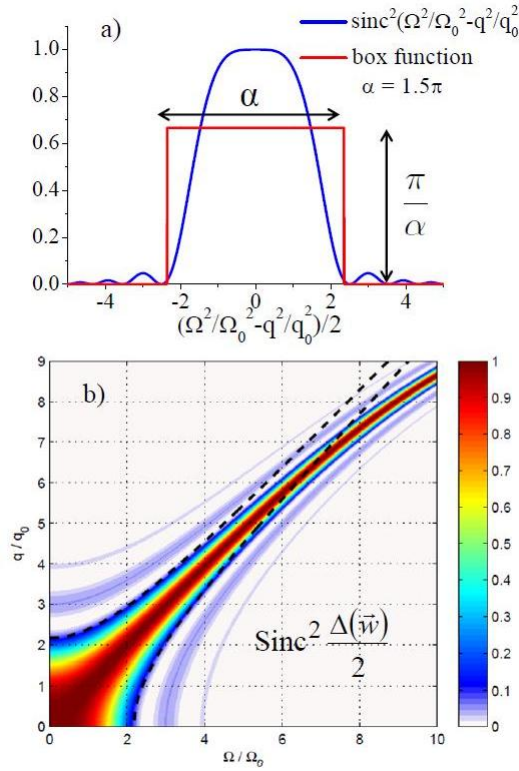


FIG. 2: a) Box function approximation (38) of the  $\text{sinc}^2$  function. b) Comparison between the true phase matching function  $|V(\vec{q}, \Omega)|^2$  and its box function approximation (boundaries of the box function are shown by dashed lines). Collinear phase matching case ( $\Delta_0 l_c = 0$ ,  $\theta_p = 22.934^\circ$ ,  $l_c = 4\text{mm}$ ).

- **large bandwidth result** ( $\bar{\Omega}_{max} > \sqrt{\alpha}$ )

$$\mathcal{K} = \frac{\alpha}{2} \sqrt{\frac{\alpha}{\pi}} q_0^2 \Omega_0 \sigma_p^2 \tau_p \left( \frac{\bar{\Omega}_{max}}{\sqrt{\alpha}} - \frac{1}{3} \right), \quad (42)$$

First of all we observe that the condition on the bandwidth can be roughly reformulated as  $\Omega_{max}$  being smaller or bigger than the characteristic GVD bandwidth  $\Omega_0$  (since  $\alpha$  is on the order of unity). The small bandwidth case corresponds to the situation where the portion of PDC emission intercepted by the measurement lies within the central region of the phase matching curve (see Fig.1), where the phase matching has no hyperbolic structure. Eqs. (41), (42) tell us that in both cases the Schmidt number is proportional to the number of modes contained in a unit volume of the phase matching region:

$$\mathcal{K} \propto \frac{\pi q_0^2 \Omega_0 \sigma_p^2 \tau_p}{8} = \frac{\pi q_0^2 \Omega_0}{\delta \vec{q}_p^2 \delta \Omega_p} \quad (43)$$

However, as the detected bandwidth increases beyond the GVD bandwidth  $\Omega_0$ , the hyperbolic geometry of phase matching enters to play, and the Schmidt number result of Eq.(42) shows a linear increase with the bandwidth.

We remind that the analytical expressions (41) and (42) estimate the Schmidt number within the NPWPA and the quadratic approximation, expressed by the condition (28) and (35), respectively. In order to verify its validity, and at the same time provide a numerical estimation of  $\mathcal{K}$  in regions of the parameter space where the NPWPA does not hold, we performed a numerical evaluation of the general expression of  $\mathcal{K}$  given by Eq.(21),(13) and (23). As it involves a 6-dimensional integral for the evaluation of  $N$  and a 12-dimensional integral for the evaluation of  $B$ , the use of a Montecarlo integration is mandatory. We used the well known method of importance sampling [26] with the aim of improving the efficiency of the Montecarlo algorithm by increasing the density of the sampled points where the functions under the integrals are larger. A natural choice has been to sample some of the Fourier variables (namely the "pump" variables in Eq.(B5)) according to Gaussian distributions coincident with the Gaussian pump spectral amplitude (27), which in the NPWPA represents the narrowest factor of the the biphoton amplitude in Eq.(24). The



implemented algorithm, very efficient for narrow spectral pump profiles, allows the evaluation of B and N even in the region where the NPWP approximation fails. No other substantial approximations are introduced, as the phase matching function is here evaluated by means of the empirical Sellmeier formulas [27].

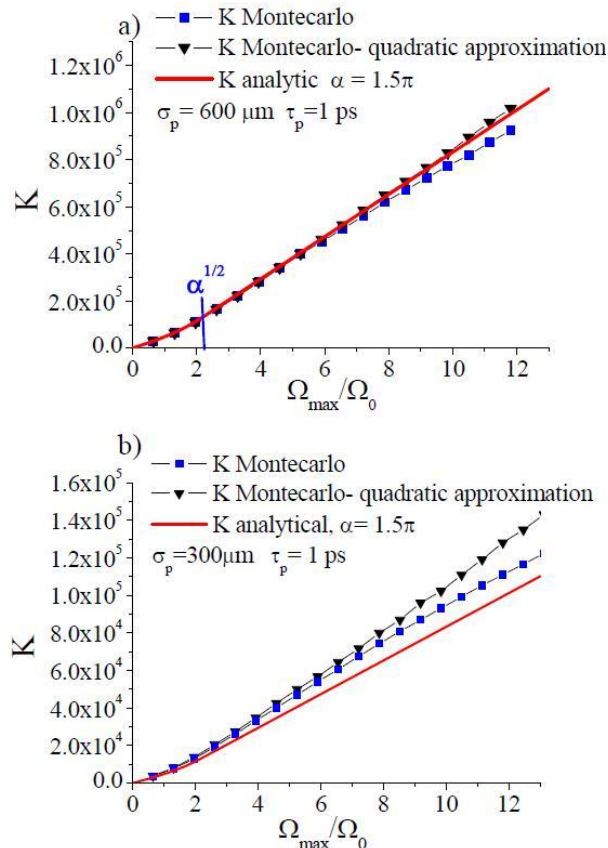


FIG. 3: Schmidt number results. Comparison between the analytic formula (41), (42) (solid red line) and Monte Carlo simulations, without any approximation (square) and with quadratic approximation (triangles). a) Pump parameters are within the NPWA b) Focused pump, beyond the NPWA. Collinear phase matching ( $\Delta_{0l_c} = 0$ ,  $\theta_p = 22.934^\circ$ ),  $l_c = 4\text{mm}$ .

Fig. 3 compares the analytic result (41), (42) with the Monte Carlo numerics, performed both without approximation (squares) and with the quadratic approximation for phase matching (triangles). Part a) of the Figure is plotted for parameters of the pump within the NPWP approximation (although very reasonable for an experimental realization) and shows an excellent agreement between the analytical curve and the numerics, in the range of validity of the quadratic approximation. Indeed, the analytic result follows very well a Monte Carlo simulation performed with the quadratic approximation, showing that the box function approximation captures the basic geometrical properties of the phase matching function. In plot b) the pump beam is more focused and as expected the analytic result deviates from numerics because of the failure of the NPWP approximation.

Monte Carlo calculations permit to obtain results also in the region of parameters beyond the NPWP approximation. Figure 4 plots the Schmidt number as a function of the parameter  $\beta = \delta q_p^2 \delta \Omega_p / q_0^2 \Omega_0$ . The NPWPA approximation is valid only for  $\beta \ll 1$ , i.e. when the widths  $\delta \Omega_p$ ,  $\delta q_p$  of the pump Fourier profile are much smaller than the characteristic scales of variation of phase matching  $\Omega_0$ ,  $q_0$ , respectively<sup>3</sup>. The Monte Carlo result shows a decrease of the Schmidt number as  $1/\beta$  for  $\beta \ll 1$ , as predicted by the analytic result (42) in the NPWPA (red solid line in the Figure). However, after reaching a minimum the Schmidt number increases again almost linearly with  $\beta$ . This behaviour is very similar to the one predicted in a purely spatial model of PDC in Ref.[9] and can be understood as follows: for

<sup>3</sup> Actually the limits of validity of the NPWPA expressed by (29) and (30) are typically much more restrictive than  $\beta \ll 1$ . For example for the BBO crystal here considered  $\delta q_p < q_0$  implies roughly  $\sigma_p > 2l_{diff} = 2/q_0 \approx 40\mu\text{m}$ , while  $\delta \Omega_p < \Omega_0$  implies  $\tau_p > 2\tau_{GVD} = 2/\Omega_0 \approx 26\text{fs}$ .

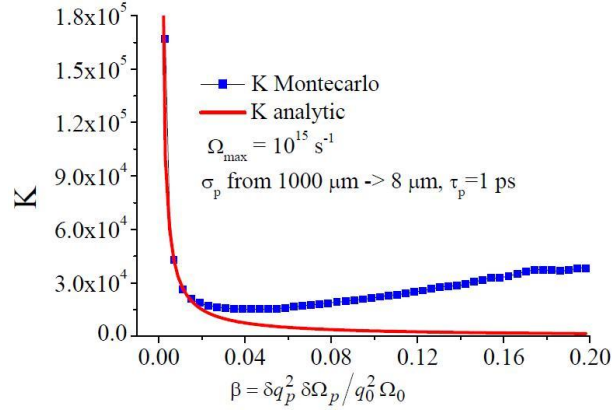


FIG. 4: Schmidt number as a function of  $\beta = \delta q_p^2 \delta \Omega_p / q_0^2 \Omega_0$ . The blue squares plot the result of a Montecarlo calculation, without any approximation, and shows that  $\mathcal{K}$  after reaching a minimum increases again almost linearly with  $\beta$ . The red solid line is the analytic result, decreasing as  $1/\beta$  (see Eq.(42), valid only within the NPWPA (small  $\beta$ ). Collinear phase matching ( $\Delta_0 l_c = 0$ ,  $\theta_p = 22.934^\circ$ ),  $l_c = 4\text{mm}$ .

a broad pump, when the NPWPA is valid, the width of the correlation is determined by the pump Fourier profile, and the number of spatio temporal modes can be estimated as in formula (34) as being proportional to the volume of phase matching divided by the pump spectral volume  $\mathcal{K} \propto q_0^2 \Omega_0 / \delta q_p^2 \delta \Omega_p = \frac{1}{\beta}$ . For a very focused pump, instead, the phase matching function in the  $\vec{q}$  direction has a smaller scale of variation than the pump Fourier spatial profile, so that the width of correlation is rather determined by the characteristic width  $\vec{q}_0$  of phase matching, and we can suppose that the number of modes is now  $\mathcal{K} \propto \delta q_p^2 / q_0^2 \propto \beta$ .

## V. FACTORABILITY OF THE SCHMIDT NUMBER IN ITS TEMPORAL AND SPATIAL COMPONENTS

In the literature the Schmidt dimensionality of twin photons is often calculated within models of PDC restricted to the spatial or the temporal domain (see [4, 5, 9, 10]. The non-factorable character of the spatio-temporal correlation demonstrated in [18, 19] suggests us that the full 3D spatio-temporal Schmidt number is not trivially given by the product of the spatial 2D and the temporal 1D Schmidt numbers. In this section we would like to understand this point.

To this end we consider models for PDC in lower dimensionalities, and follow the same procedure outlined in the previous sections to calculate the Schmidt number. The purely spatial 2D model is obtained by neglecting the temporal coordinate and setting  $\Omega = 0$ . Similarly the purely temporal 1D model neglects the spatial coordinates and sets  $\vec{q} = 0$ . The starting point of the analysis is in both cases the general integral formula for the Schmidt number (21) where we have now to interpret the Fourier coordinates as:

$$\vec{w} = \begin{cases} \Omega \in \mathcal{R} & \text{in } 1D \\ \vec{q} \in \mathcal{R}^2 & \text{in } 2D \\ \vec{q}, \Omega \in \mathcal{R}^3 & \text{in } 3D \end{cases} \quad (44)$$

Similarly, in the expression involving the coordinates in the direct space:

$$\vec{\xi} = \begin{cases} t \in \mathcal{R} & \text{in } 1D \\ \vec{x} \in \mathcal{R}^2 & \text{in } 2D \\ \vec{x}, t \in \mathcal{R}^3 & \text{in } 3D \end{cases} \quad (45)$$

For example, by introducing the NPWP approximation in the various models (clearly NPWPA in the spatial model means that the pump has a broad waist, while the temporal model assumes a long enough pulse duration), we obtain the NPWPA expression for the Schmidt number in an arbitrary D-dimensional model:

$$\mathcal{K} = \frac{\left[ \int d\vec{\xi}_p |\mathcal{A}_p(\vec{\xi}_p)|^2 \right]^2}{\int d\vec{\xi}_p |\mathcal{A}_p(\vec{\xi}_p)|^4} \frac{\left[ \int d\vec{w} |V(\vec{w})|^2 \right]^2}{(2\pi)^D \int d\vec{w} |V(\vec{w})|^4}. \quad (46)$$

### A. Spatial Schmidt number $\mathcal{K}_{2D}$

By performing calculations similar to those reported for the 3D model, we derive an expression for the Schmidt number in the purely spatial case, valid within the NPWPA and the quadratic approximation for phase matching. The latter one corresponds to approximating the phase matching function as

$$\Delta_{2D}(\vec{q}) = k_s(\vec{q}) + k_s(-\vec{q}) - k_p \approx \frac{q^2}{q_0^2} \quad (47)$$

In the 2D case the result depends on the spatial bandwidth  $\bar{q}_{max} = q_{max}/q_0$  intercepted by the measurement:

$$\mathcal{K}_{2D} = \frac{3}{8}\pi\sigma_p^2 q_0^2 \frac{\bar{q}_{max}^2}{\alpha} \quad \bar{q}_{max} < \sqrt{\alpha} \quad (48)$$

$$\mathcal{K}_{2D} = \frac{3}{8}\pi\sigma_p^2 q_0^2 \quad \bar{q}_{max} > \sqrt{\alpha} \quad (49)$$

where we remind that  $\alpha \approx 1.5\pi$ . In Fig.5 this curve is compared with an exact Montecarlo calculation performed

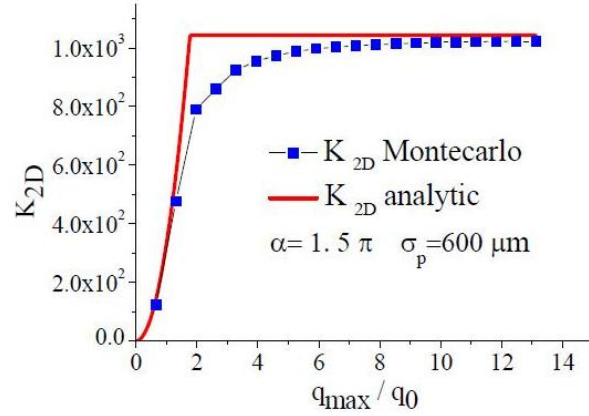


FIG. 5: 2D spatial Schmidt number  $\mathcal{K}_{2D}$  as a function of the collected spatial bandwidth  $q_{max}$ . The solid red line is the analytic result (48), (49), the squares plot the Monte Carlo numeric result. The waist of the pump beam is  $\sigma_p = 600\mu\text{m}$ .

in the 2D model. Beyond noticing that the two results agree qualitatively, we remark that, differently from the 3D case, the 2D Schmidt number saturates to the maximum value  $\mathcal{K}_{2Dmax} = \frac{3}{8}\pi\sigma_p^2 q_0^2 = \frac{3}{8}\pi q_0^2 / \delta q_p^2$ . This behaviour can be explained with the help of the geometrical interpretation (34), valid in the NPWPA, which evaluates the Schmidt number as the ratio between the volume of the phase matching region and the correlation volume. In the 2D case phase matching is described by Eq. (47), so that in the  $(q_x, q_y)$  plane phase matching occurs within a circle of area  $\approx \pi q_0^2$ . For increasing  $q_{max}$ , the PDC photons are detected in increasing large circular regions, so that the Schmidt number increases quadratically with  $q_{max}$  until the border of the phase matching region  $q_{max} = q_0\sqrt{\alpha}$  is reached.

### B. Temporal Schmidt number $\mathcal{K}_{1D}$

We now consider the purely temporal model of PDC, by setting  $\vec{q} = 0$ . We perform again analytic calculation in the NPWPA and the quadratic approximation for phase matching, that in the 1D case reads

$$\Delta_{1D}(\Omega) = k_s(\Omega) + k_s(-\Omega) - k_p \approx \frac{\Omega^2}{\Omega_0^2} \quad (50)$$

The analytic expression for  $\mathcal{K}_{1D}$  in these limits, obtained by using the box function approximation, depends on the collected temporal bandwidth  $\bar{\Omega}_{max} = \Omega_{max}/\Omega_0$ :

$$\mathcal{K}_{1D} = \sqrt{\frac{\alpha}{\pi}} \tau_p \Omega_0 \frac{\bar{\Omega}_{max}}{\sqrt{\alpha}} \quad \bar{\Omega}_{max} < \sqrt{\alpha} \quad (51)$$

$$\mathcal{K}_{1D} = \sqrt{\frac{\alpha}{\pi}} \tau_p \Omega_0 \quad \bar{\Omega}_{max} > \sqrt{\alpha} \quad (52)$$

Figure 6 plots this analytical result together with the exact Montecarlo 1D calculation. Also in this case, similarly to the 2D case, the Schmidt number saturates to the maximum value  $\mathcal{K}_{1Dmax} \approx \tau_p \Omega_0$ , because phase matching occurs only inside an interval of size  $\approx \Omega_0$ , so that by increasing  $\Omega_{max}$  beyond the critical value  $\sqrt{\alpha}\Omega_0$ , we begin to consider regions where there is no phase matching, which do not contribute to the integral.

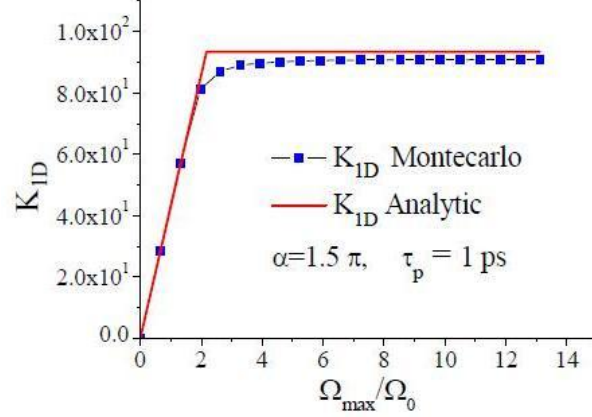


FIG. 6: 1D temporal Schmidt number  $\mathcal{K}_{1D}$  as a function of the maximum temporal frequency  $\Omega_{max}$ . The solid line shows the analytic result (within the NPWA and quadratic approximation), the squares plot the numeric exact result. Pump time duration  $\tau_p = 1$ ps.

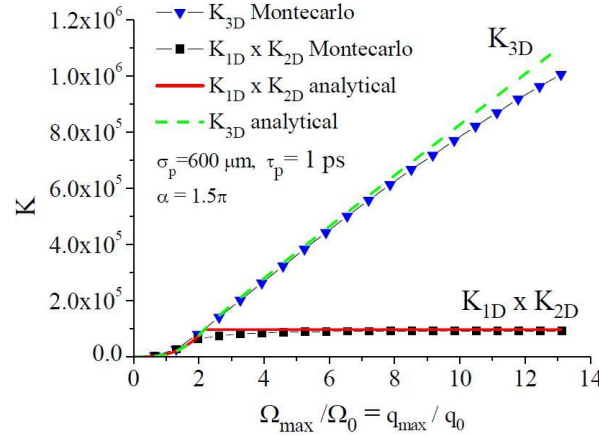


FIG. 7: Comparison between the Schmidt number  $\mathcal{K}$  calculated in the full spatio-temporal model and the product of the Schmidt numbers  $\mathcal{K}_{1D} \times \mathcal{K}_{2D}$ , calculated in the purely 1D temporal and 2D spatial models. The abscissa is the collected temporal bandwidth, set equal to the spatial bandwidth in normalized units. Lines plot analytic results, symbols provide the Montecarlo results.

### C. Comparison

We are now in conditions of comparing the results obtained in the models of various dimensionalities. To this end, we have to reformulate slightly the 3D problem. In SectionIV we calculated  $\mathcal{K}$  as a function of the collected temporal bandwidth by assuming that no selection on the spatial bandwidth was performed, i.e.  $\bar{q}_{max} = \infty$ . This is a possible correct choice to present results, but in order to have a clean comparison with the 2D and 1D models, we need also to limit the detected spatial bandwidth. The simplest possibility is to set  $\bar{q}_{max} = \Omega_{max}$ . This choice is justified by the fact that in the quadratic approximation, phase matching is realized along the lines  $\frac{q}{q_0} = \pm \frac{\Omega}{\Omega_0}$  so that by increasing simultaneously the spatial and temporal bandwidth  $\frac{q_{max}}{q_0} = \frac{\Omega_{max}}{\Omega_0}$  one follows the phase matching curve.

With this in mind, analytical calculations in the PWA, quadratic approximation for phase matching and box function approximation can be performed. The result for the 3D Schmidt number is plotted in Fig.7 (dashed line) together with the Montecarlo exact result (triangles). In the same figure we compare these 3D results with the product of the Schmidt numbers obtained in the models with lower dimensionalities i.e.  $\mathcal{K}_{2d} \times \mathcal{K}_{1D}$ . From these plots it clearly emerges that the factorizability holds only when the detected bandwidth is small, i.e. when both  $q_{max}$  and  $\Omega_{max}$  lie within the phase matching bandwidths  $q_0$ ,  $\Omega_0$ , respectively. However, as the detected bandwidth gets larger, the

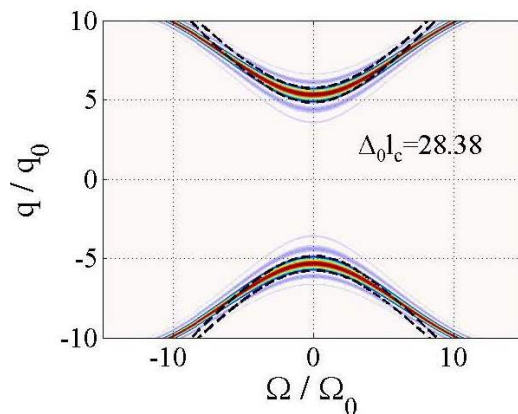


FIG. 8: Colormap plot of  $|V(\vec{q}, \Omega)|^2$  in the non-collinear phase matching case,  $\Delta_0 l_c > 0$ , ( $\Delta_0 l_c = 23.38$ ). The dashed lines are the boundaries of the box function, where  $\Delta(\vec{q}, \Omega) = \pm\alpha$

result in the fully 3D spatiotemporal model grows linearly with the detected bandwidth, and diverges clearly from the product  $\mathcal{K}_{2d} \times \mathcal{K}_{1D}$  which saturates to a fixed value  $\propto q_0^2 \Omega_0$ . This result can be easily understood with the help of the geometrical interpretation of the Schmidt number as the number of entangled modes contained in the phase matching region: close to the degeneracy and to the collinear emission, the phase matching region can be seen as a spherical region, which obviously factorizes in the spatial and temporal components, so that the number of spatio-temporal modes is trivially the product of the numbers of spatial and temporal modes times. Conversely, if the collected bandwidth is large enough, than the biconical, non-factorizable geometry of phase matching comes into play, so that a full 3D model has to be used to correctly compute the number of spatio-temporal modes.

## VI. ENTANGLEMENT WITHOUT PHASE MATCHING

Up to now we considered the case of collinear phase matching ( $\Delta_0 l_c = 0$ ), characterized by the fact that exact phase matching  $\Delta(\vec{w}) = 0$  can be realized for any value of the transverse wave-vector of the photon pair, such that  $q/q_0 = \pm\Omega/\Omega_0$ . However, if the crystal is tuned away from the collinear conditions ( $\Delta_0 l_c \neq 0$ ), there exist regions of the  $(\vec{q}, \Omega)$  space where phase matching does not occur at all. In these regions, the probability of emission of photon pairs is low, although not zero.

In particular, we focus on the case of non-collinear phase matching ( $\Delta_0 l_c > 0$ ). Fig.8 shows the typical behaviour of the phase matching function  $\text{sinc}^2(\Delta(\vec{w})/2)$ . From the quadratic expansion of the phase mismatch

$$\Delta(q, \Omega) \approx \Delta_0 l_c - \frac{q^2}{q_0^2} + \frac{\Omega^2}{\Omega_0^2}, \quad (53)$$

we immediately realize that phase matching does not occur for modes close to collinear emission, namely having  $|\vec{q}| < \sqrt{\Delta_0 l_c}$

We have calculated the 3D spatio-temporal Schmidt number in these conditions: Fig. 9 plots the result as a function of the collected spatial bandwidth  $q_{max}$ . We find that for small bandwidths, such that the collected photons are not phase matched, the degree of entanglement is very high, actually larger than in the region where phase matching is realized. This result is apparently paradoxical, because in the absence of phase matching the probability of emission of a photon pair is very low and one could infer that the state should be very close to the separable vacuum state. For comparison Fig.10 displays the corresponding mean number of photons, which as expected, is indeed very low where there is no phase matching.

However, in order to understand the results of Fig. 9 we have to remind that we are studying the degree of entanglement of the state (15), conditioned to the detection of a photon pair. This means that our calculation of the Schmidt number has lost track of the presence of a large vacuum contribution to the original PDC state, and the result has to be interpreted as *photon pairs are emitted with very low probability, however, when a pair is detected it is highly entangled*.

The point to understand is therefore why the non-phase matched photon pairs are more entangled than the phase matched ones. The Schmidt number  $\mathcal{K} = 1/\sum_j \lambda_j^2$  provides an estimate of the number of significant eigenvalues of

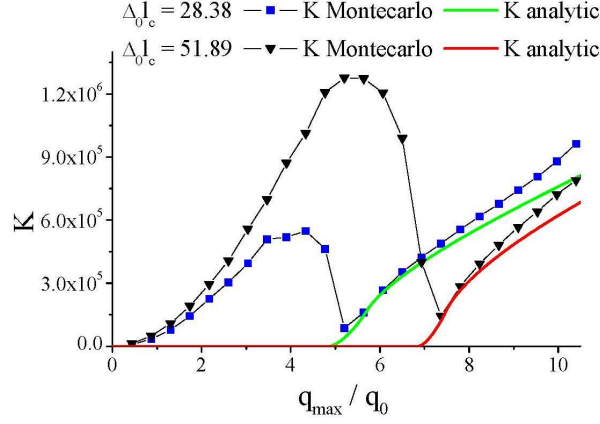


FIG. 9: Schmidt number  $\mathcal{K}$  in the non-collinear phase matching case, as a function of the collected spatial bandwidth  $q_{max}$ , normalized to the diffraction bandwidth  $q_0$ . Parameters are  $\sigma_p = 600\mu\text{m}$ ,  $\tau_p = 1\text{ps}$

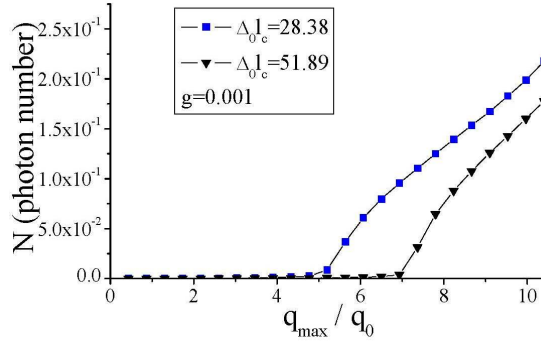


FIG. 10: Number of photons  $N$  in the non-collinear case, as a function of  $\bar{q}_{max}$ . Parameters are  $\sigma = 600\mu\text{m}$ ,  $\tau_p = 1\text{ps}$ ,  $g = 0.001$ .

the Schmidt decomposition, i.e. the number of entangled eigenmodes that participate to the modal decomposition. In the region where no phase-matching occurs (for  $\bar{q}_{max} < \sqrt{\Delta_0 l_c}$ ),  $\mathcal{K}$  can be in practice very large, since there is no mechanism for modal selection and all the modes in the collected bandwidth participate equally to the PDC process even though with a very low occupation probability. By contrast, when increasing  $\bar{q}_{max}$  towards  $\sqrt{\Delta_0 l_c}$  and entering the phase-matching region, a strongly reduced number of phase-matched spatio-temporal modes contribute to the Schmidt decomposition, the few which are close to satisfy the phase-matching condition  $\bar{q} = \sqrt{\Delta_0 l_c}$ ,  $\Omega = 0$ . The number of significant eigenmodes is therefore reduced because phase matching operates a selection of the spatio-temporal modes that efficiently participate to the entanglement of the state. In other terms, the phase-matching mechanism favors only a small number of modes, reducing thereby drastically the dimensionality of the entangled state. By increasing  $\bar{q}_{max}$  above  $\sqrt{\Delta_0 l_c}$  the Schmidt number  $\mathcal{K}$  starts again to increase, according to the geometrical interpretation of the Schmidt number as being proportional again to the phase matching volume

## VII. CONCLUSIONS

In this work we have calculated the Schmidt dimensionality of the two-photon state generated by PDC in the ultra-low gain regime. Results have been produced with different degrees of approximation: Monte Carlo calculations allow us to obtain the Schmidt number without relevant approximations, while when the pump beam is broad enough (NPWPA) we have demonstrated a transparent geometrical interpretation of the Schmidt number, which can be seen as the number of entangled modes contained in the region where phase matching occurs.

The same calculations have been performed in models restricted to the purely spatial or temporal degrees of freedom of biphotons. A remarkable result demonstrated is that, when the collected spatio-temporal bandwidth is large enough,

the Schmidt dimensionality of the full spatio-temporal state cannot be trivially reduced to the product of the Schmidt numbers characterizing the entanglement in lower dimensions. Therefore, obtaining the Schmidt number in the full 3D model is not a mere exercise of calculus: in order to correctly characterize the entanglement of twin photons it is necessary to consider simultaneously their spatial and temporal degrees of freedom. This result is a clear consequence of the non-factorability of the state in space and time, and mirrors the findings described in Refs. [18], [19] where the spatio-temporal correlation of the biphoton state was shown to have a non factorable X-shaped geometry.

The non-factorability has been demonstrated in this work only in the NPWPA. Question is still open whether in the opposite limit, that is, for a very focused and short pump pulse, the Schmidt number keeps the non-factorable character, and it is obviously linked to the more general question whether the state appears to be factorable in space and time in these conditions. We however remark that reaching this limit is in practice very demanding, because it requires that the pump Fourier profile **at the exit face of the crystal** is much broader than the width of the phase matching function. For a few millimeter crystal, this implies a pump waist on the order of tens of microns, and a pulse duration as short as few tens of femtosecond. While the first condition could be in principle achieved by strongly focusing at the end face of the crystal, the second is more demanding because of dispersion occurring inside the nonlinear material.

An intriguing finding is that in the absence of phase matching, where the probability of emission of photon pair is very low, the Schmidt dimensionality of the state is huge, actually larger than in the regions where phase matching occurs. This counter-intuitive finding has been explained through the mode selection mechanism performed by phase matching, which reduces the available number of spatio-temporal modes. However, in evaluating this result and its usefulness for applications, one has to remember that the Schmidt number here analysed does not refer to the full PDC state, but to the state conditioned to the detection of a photon pair.

### Acknowledgments

We acknowledge support from the Fet Open programme of the EC within the grant 221906 HIDEAS *High Dimensional Entangled Systems*

### Appendix A: Partial density matrix

In order to calculate the partial trace of the density matrix (18) it is enough to consider the vacuum state  $|0\rangle_2$  of the "idler" subsystem 2, plus the continuous set of 1 photon states

$$\left\{ A_2^\dagger(\vec{w}_2) |0\rangle_2 \right\} \quad (\text{A1})$$

It is convenient to write the density matrix (18) as

$$\rho = \frac{1}{N} M^\dagger |0\rangle \langle 0| M \quad (\text{A2})$$

where  $M$  is the operator that annihilates a photon pair in any spatiotemporal mode (weighted by  $\psi$ )

$$M = \int d\vec{w}_1 \int d\vec{w}_2 \psi^*(\vec{w}_1, \vec{w}_2) A_1(\vec{w}_1) A_2(\vec{w}_2) \quad (\text{A3})$$

We then have

$$\begin{aligned} \rho_1 &= \text{Tr}_2\{\rho\} \\ &= \frac{1}{N} \left\{ {}_2\langle 0| M^\dagger |0\rangle_2 {}_1\langle 0| {}_2\langle 0| M |0\rangle_2 + \int d\vec{w}_3 {}_2\langle 0| A_2(\vec{w}_3) M^\dagger |0\rangle_2 {}_1\langle 0| {}_2\langle 0| M A_2^\dagger(\vec{w}_3) |0\rangle_2 \right\} \quad (\text{A4}) \end{aligned}$$

$$\begin{aligned} &= \frac{1}{N} \left\{ \int d\vec{w}_3 \int d\vec{w}_1 \int d\vec{w}_2 \int d\vec{w}'_1 \int d\vec{w}'_2 \psi(\vec{w}_1, \vec{w}_2) \psi^*(\vec{w}'_1, \vec{w}'_2) \right. \\ &\times \left. {}_2\langle 0| A_2(\vec{w}_3) A_2^\dagger(\vec{w}_2) |0\rangle_2 A_1^\dagger(\vec{w}_1) |0\rangle_1 {}_1\langle 0| A_1(\vec{w}'_1) {}_2\langle 0| A_2(\vec{w}_2) A_2^\dagger(\vec{w}_3) |0\rangle_2 \right\} \quad (\text{A5}) \end{aligned}$$

$$= \frac{1}{N} \left\{ \int d\vec{w}_1 \int d\vec{w}_2 \int d\vec{w}'_1 \psi(\vec{w}_1, \vec{w}_2) \psi^*(\vec{w}'_1, \vec{w}_2) A_1^\dagger(\vec{w}_1) |0\rangle_1 {}_1\langle 0| A_1(\vec{w}'_1) \right\} \quad (\text{A6})$$

$$= \frac{1}{N} \left\{ \int d\vec{w}_1 \int d\vec{w}'_1 G(\vec{w}'_1, \vec{w}_1) A_1^\dagger(\vec{w}_1) |0\rangle_1 {}_1\langle 0| A_1(\vec{w}'_1) \right\} \quad (\text{A7})$$

where in passing from (A5) to (A6) we used the relation

$${}_2\langle 0 | A_2(\vec{w}_2) A_2^\dagger(\vec{w}'_2) | 0 \rangle_2 = \delta(\vec{w}_2 - \vec{w}'_2) \quad (\text{A8})$$

which comes directly from the commutation rules of bosonic operators.

### Appendix B: Derivation of formula (31)

We wish here to simplify the general formula (21) by exploiting the NPWPA introduced in Section III (see Eq.(28)). We rewrite formula (21) as

$$\mathcal{K} = \frac{N'^2}{B'} \quad (\text{B1})$$

with

$$B' = \int d\vec{w}_1 \int d\vec{w}_2 \int d\vec{w}'_1 \int d\vec{w}'_2 \tilde{\mathcal{A}}_p(\vec{w}_1 + \vec{w}_2) \tilde{\mathcal{A}}_p(\vec{w}'_1 + \vec{w}'_2) \tilde{\mathcal{A}}_p^*(\vec{w}'_1 + \vec{w}_2) \tilde{\mathcal{A}}_p^*(\vec{w}'_1 + \vec{w}_2) \cdot V(\vec{w}_1, \vec{w}_2) V(\vec{w}'_1, \vec{w}'_2) V^*(\vec{w}'_1, \vec{w}_2) V^*(\vec{w}_1, \vec{w}'_2); \quad (\text{B2})$$

$$N' = \int d\vec{w}_1 d\vec{w}_2 |\tilde{\mathcal{A}}_p(\vec{w}_1 + \vec{w}_2)|^2 |V(\vec{w}_1, \vec{w}_2)|^2. \quad (\text{B3})$$

where we inserted the explicit expression (24) for the biphoton amplitude (without a constant coefficient). Here the function  $V$  depends on phase matching and is given by Eq.(25), while  $\tilde{\mathcal{A}}_p$  is the Fourier profile of the pump. We start by simplifying the integral  $B'$  in Eq.(B2), by introducing the change of variables

$$(\vec{w}_1, \vec{w}'_1, \vec{w}_2, \vec{w}'_2) \rightarrow (\vec{w}_1, \vec{\delta} = \vec{w}_1 - \vec{w}'_1, \vec{w}_p = \vec{w}_1 + \vec{w}_2, \vec{w}'_p = \vec{w}'_1 + \vec{w}'_2) \quad (\text{B4})$$

With this change,  $B'$  becomes

$$B' = \int d\vec{w}_p d\vec{w}'_p d\vec{\delta} d\vec{w}_1 \tilde{\mathcal{A}}_p(\vec{w}_p) \tilde{\mathcal{A}}_p(\vec{w}'_p) \tilde{\mathcal{A}}_p^*(\vec{w}_p - \vec{\delta}) \tilde{\mathcal{A}}_p^*(\vec{w}'_p + \vec{\delta}) V(\vec{w}_1, -\vec{w}_1 + \vec{w}_p) V(\vec{w}_1 - \vec{\delta}, -\vec{w}_1 + \vec{\delta} + \vec{w}'_p) V^*(\vec{w}_1 - \vec{\delta}, -\vec{w}_1 + \vec{w}_p) V^*(\vec{w}_1, -\vec{w}_1 + \vec{\delta} + \vec{w}'_p). \quad (\text{B5})$$

In this expression the variables  $\vec{w}_p$  and  $\vec{w}'_p$  die on the scale of the inverse of the pump waist/duration, i.e.  $(2/\sigma_p, 2/\tau_p)$ . Because of the presence of the terms  $\tilde{\mathcal{A}}_p^*(\vec{w}'_p - \vec{w}_1 + \vec{w}_p)$  and  $\tilde{\mathcal{A}}_p^*(\vec{w}_1 - \vec{w}'_p + \vec{w}'_p)$ , also the variable  $\vec{\delta} = \vec{w}_1 - \vec{w}'_1$  dies out on the same scale. We can then make use of the NPWP approximation, which amounts to substituting

$$\begin{aligned} V(\vec{w}_1, -\vec{w}_1 + \vec{w}_p) &\approx V(\vec{w}_1 - \vec{\delta}, -\vec{w}_1 + \vec{\delta} + \vec{w}'_p) \\ &\approx V(\vec{w}_1, -\vec{w}_1) := V(\vec{w}_1) \end{aligned} \quad (\text{B6})$$

where we took into account that all the pump variables  $\vec{w}_p$ ,  $\vec{\delta}$ ,  $\vec{\delta} + \vec{w}'_p$  dies out on the fast scale of the inverse of the pump waist/duration, over which the function  $V$  remains constant. Similarly

$$\begin{aligned} V^*(\vec{w}_1 - \vec{\delta}, -\vec{w}_1 + \vec{w}_p) &\approx V^*(\vec{w}_1, -\vec{w}_1 + \vec{\delta} + \vec{w}'_p) \\ &\approx V^*(\vec{w}_1, -\vec{w}_1) := V^*(\vec{w}_1) \end{aligned} \quad (\text{B7})$$

Within the NPWP approximation we hence obtain a new expression for  $B'$ , which reads:

$$B' = \int d\vec{w}_p d\vec{w}'_p d\vec{\delta} \tilde{\mathcal{A}}_p(\vec{w}_p) \tilde{\mathcal{A}}_p(\vec{w}'_p) \tilde{\mathcal{A}}_p^*(\vec{w}_p - \vec{\delta}) \tilde{\mathcal{A}}_p^*(\vec{w}'_p + \vec{\delta}) \times \int d\vec{w}_1 |V(\vec{w}_1)|^4. \quad (\text{B8})$$

The integral over the pump variables can be further simplified by noting that it involves two convolutions:

$$\int d\vec{w}_p \tilde{\mathcal{A}}_p(\vec{w}_p) \tilde{\mathcal{A}}_p^*(\vec{w}_p \pm \vec{\delta}) = \int d\vec{\xi}_p |\mathcal{A}_p(\vec{\xi}_p)|^2 e^{-\pm i\vec{\xi}_p \cdot \vec{\delta}} = (2\pi)^{\frac{3}{2}} [\mathcal{F}(|\mathcal{A}_p|^2)](\pm\vec{\delta}), \quad (\text{B9})$$

where the symbol  $\mathcal{F}(f)$  denotes the Fourier transform of the function  $f$ . By performing also the integration over  $\vec{\delta}$  we obtain

$$\int d\vec{\delta} [\mathcal{F}(|\mathcal{A}_p|^2)](\vec{\delta}) [\mathcal{F}(|\mathcal{A}_p|^2)](-\vec{\delta}) = \int d\vec{\xi}_p |\mathcal{A}_p(\vec{\xi}_p)|^4, \quad (\text{B10})$$



where we used the Plancherel theorem  $\int d^3\vec{w}|\tilde{f}(\vec{w})|^2 = \int d^3\xi|f(\xi)|^2$ . This leads to:

$$B' = (2\pi)^3 \left[ \int d\vec{\xi}_p |\mathcal{A}_p(\vec{\xi}_p)|^4 \right] \left[ \int d\vec{w} |V_{pw}(\vec{w})|^4 \right]. \quad (\text{B11})$$

In order to complete the Schmidt number calculation we also have to evaluate  $N'$ , proportional to the mean photon number. With the usual change of variables  $(\vec{w}_1, \vec{w}_2) \rightarrow (\vec{w}_p = \vec{w}_1 + \vec{w}_2, \vec{w}_1)$ , equation (B3) becomes:

$$N' = \int d\vec{w}_p |\tilde{\mathcal{A}}_p(\vec{w}_p)|^2 \int d\vec{w}_1 |V(\vec{w}_1, -\vec{w}_1 + \vec{w}_p)|^2. \quad (\text{B12})$$

In the NPWP limit (see Eq. 28) we get

$$N' = \int d\vec{w}_p |\tilde{\mathcal{A}}_p(\vec{w}_p)|^2 \int d\vec{w} |V(\vec{w})|^2, \quad (\text{B13})$$

which, using the Plancherel theorem in the first integral, can be also written as

$$N' = \int d\vec{\xi}_p |\tilde{\mathcal{A}}_p(\vec{\xi}_p)|^2 \int d\vec{w} |V(\vec{w})|^2. \quad (\text{B14})$$

In NPWP limit the Schmidt number takes therefore the symplified form

$$\mathcal{K} = \frac{N^2}{B} = \frac{\left[ \int d\vec{\xi}_p |\mathcal{A}_p(\vec{\xi}_p)|^2 \right]^2}{\int d\vec{\xi}_p |\mathcal{A}_p(\vec{\xi}_p)|^4} \frac{\left[ \int d\vec{w} |V(\vec{w})|^2 \right]^2}{(2\pi)^3 \int d\vec{w} |V(\vec{w})|^4} \quad (\text{B15})$$

where the integrals now factorize into the pump and signal degrees of freedom.

- 
- [1] see e.g. the website of the project HIDEAS at <http://hideas.dfm.uninsubria.it/>, and the papers listed there
- [2] A. Ekert, P.L. Knight, American Journal of Physics, **63**, 415-423 (1995)
- [3] S. Parker, S. Bose, and M. B. Plenio, Phys. Rev. A, **61**, 032305 (2000).
- [4] C.K Law, I.A. Walmsley and J.H. Eberly, Phys. Rev. Lett **84** 5304 (2000)
- [5] Yu. M. Mikhailova, P. A. Volkov, and M. V. Fedorov, Phys. Rev. A **78**, 062327 (2008)
- [6] G. Patera, G. De Valcarcel, N. Treps, C. Fabre, Europ. Phys. J. D **56**, 123 (2010).
- [7] O. Pinel, Pu Jian, R. Medeiros, Jinxia Feng, B; B. Chalopin, C. Fabre, N. Treps, Phys. Rev. Lett. **108**, 083601 (2012), arXiv:1103.6123v2 [quant-ph].
- [8] Malte Avenhaus, Maria V. Chekhova, Leonid A. Krivitsky, Gerd Leuchs and Christine Silberhorn, Phys. Rev. A **79**, 043836 (2009)
- [9] C.K Law, and J.H. Eberly, Phys. Rev. Lett **92** 127903 (2004)
- [10] M.P Van Exter, A. Aiello, S.S.R. Oemrawsingh, G. Nienhuis and J.P. Woerdman, Phys. Rev. Lett **74** 5304 (2006)
- [11] J. P. Torres, A. Alexandrescu, and Lluís Torner, Phys. Rev. A **68**, 050301(R) (2003).
- [12] Gabriel Molina-Terriza, Juan P. Torres, Lluís Torner, Nature Physics **3**, 305 - 310 (2007)
- [13] Sonja Franke-Arnold, Les Allen, and Miles Padgett Laser and Photonics Reviews **2**, 299-313 (2008)
- [14] A.C. Dada, J. Leach, G.S. Buller, GS (Buller, M.J. Padgett, E. Andersson, Nature Physics **7**, 677-680 (2011)
- [15] H. Di Lorenzo Pires, C.H. Monken, M.P. van Exter, Phys. Rev. A **80**, 022307 (2009)
- [16] H. Di Lorenzo Pires, H.C.B. Florijn and M.P. van Exter, Phys. Rev. Lett. **104**, 020505 (2010).
- [17] see e.g. A. Gatti, E. Brambilla, L. Lugiato, Quantum Imaging in Progress in Optics **51**, pp.251-348, E. Wolf editor (2008, Elsevier B.V. Amsterdam)
- [18] A. Gatti, E. Brambilla, L. Caspani and L. Lugiato, Phys. Rev. Lett. **102**, 223601 (2009).
- [19] L. Caspani, E. Brambilla and A. Gatti, Phys. Rev. A **81**, 033808 (2010)
- [20] E. Brambilla, L. Caspani, L.A. Lugiato and A. Gatti, Phys. Rev. A. **82**, 013835 (2010)
- [21] O. Jedrkiewicz, J.-L. Blanchet, E. Brambilla, P. Di Trapani and A. Gatti, Phys. Rev. Lett. **108**, 253904 (2012) e-print arXiv:1203.3661
- [22] Enrico Brambilla, Ottavia Jedrkiewicz, Luigi Lugiato, Alessandra Gatti, Phys. Rev. A **85**, 063834 (2012), preprint arXiv:1205.1637
- [23] Clara I Osorio, Alejandra C Valencia and Juan P Torres, New Journal of Phys. **10**, 113012 (2008)
- [24] A. Gatti, R. Zambrini, M. San Miguel, L. Lugiato, Phys. Rev. A **68**, 053807 (2003)
- [25] D.B. Horoshko, G. Patera, A. Gatti, and M.I. Kolobov, X-entangled biphotons: Schmidt number for 2D model, Europ. Phys. J. D, press (July 2012)
- [26] J. M. Hammersley and D. C. Handscorn, Monte Carlo Methods, Chapman and Hall, London & New York (1964).
- [27] V. G. Dmitriev, G. G. Gurzadyan, D. N. Nikogosyan, *Handbook of nonlinear optical crystals*, Springer series in optical sciences, Springer-Verlag, Berlin (1991); N. Boeuf et al., Optical Engineering, **39**, 1016 (2000).